

# Defect Assisted Localization of $Mn^{2+}$ Activating Ions in the Core of the ZnS Quantum Dots

S.V. NISTOR, M. STEFAN, L.C. NISTOR, D. GHICA and  
C.D. MATEESCU

National Institute of Materials Physics, Atomistilor 105 bis,  
077125 Magurele-Ilfov, Romania  
E-mail: [snistor@infim.ro](mailto:snistor@infim.ro)

**Abstract.** Multifrequency electron paramagnetic resonance (EPR) and high resolution transmission electron microscopy (HRTEM) investigations were performed on cubic ZnS:Mn quantum dots (QDs) of 2 nm, synthesized by a surfactant-assisted liquid-liquid reaction. The EPR spectra reveal the presence of  $Mn^{2+}$  ions localized substitutionally and at the surface of QDs. Based on accurate EPR spectra analysis we demonstrate that the substitutional  $Mn^{2+}$  ions are localized in the core of the ZnS QDs at  $Zn^{2+}$  sites, next to an extended lattice defect. Their presence, confirmed by HRTEM measurements, seems to be essential in the incorporation of  $Mn^{2+}$  activating ions in cubic II-VI semiconductor QDs.

## 1. Introduction

Activating impurities, in particular transition ions, play an essential role in fulfilling the expected exceptional properties of semiconducting nanocrystals. To understand the mechanisms responsible for their incorporation and the resulting quantum properties one needs to know the precise location of the doping impurities in the nanocrystals (NCs) lattice. In the case of wide band-gap nanocrystalline II-VI semiconductors, which are prepared at relatively low temperatures ( $< 350^{\circ}C$ ), such information could also help in understanding the still unclear mechanisms responsible for the incorporation of activating impurity ions such as  $Mn^{2+}$  or  $Co^{2+}$  [1, 2].

Electron paramagnetic resonance (EPR) spectroscopy can accurately determine the localization of the paramagnetic impurities and the resulting changes in the neighboring ligands configuration [3]. In the case of luminescent cubic ZnS (cZnS) NCs [4], it was for quite long accepted [1,5-10] that the substitutional  $Mn^{2+}$  ions

are localized at the cation ( $\text{Zn}^{2+}$ ) sites with local cubic  $T_d$  symmetry, similar to the case of cZnS single crystals [11]. Despite this assumption, in the publications dedicated to this subject [6-10] the spin Hamiltonian (SH) describing the EPR spectra also included, besides the cubic Zeeman and hyperfine interaction terms with parameter values centered around  $g = 2.002$  and  $|A| = 64 \times 10^{-4} \text{ cm}^{-1}$  [11], additional axial and even rhombic zero-field-splitting (ZFS) terms characterized by the  $D$  and  $E$  parameters, respectively. The corresponding reported values were spread over a two orders of magnitude range [6-10], a situation which can be explained by the low accuracy of the procedures used to determine the SH parameters and the low resolution of the experimentally obtained EPR spectra. One should also mention that no clear explanation for the presence of the reported non-cubic ZFS terms was given.

In an effort to improve this situation, we could synthesize by a surfactant-assisted liquid-liquid reaction at room temperature (RT) small cZnS NCs doped with  $\text{Mn}^{2+}$  self-assembled into a mesoporous structure with a tight size distribution, centered around 2 nm and an improved lattice quality [12, 13]. Such small size NCs, to be further called quantum dots (QDs), in which quantum confinement (QC) effects are expected to take place, exhibited EPR spectra with the smallest line-width reported so-far and a corresponding increased spectra resolution, beyond the best reported data available in the literature [14, 15]. These properties were attributed to the self-assembling.

As will be shown here, the full quantitative analysis of the resulting low and high frequency EPR spectra resulted in accurate SH parameters for the substitutional, as well as for the surface  $\text{Mn}^{2+}$  centers, which confirmed, in the case of the substitutional center, the presence of an axial ZFS term and an accurate determination of the characteristic  $D$  parameter value. Moreover, by comparing the resulting spectral parameters with those reported in early experimental investigations concerning EPR parameters of  $\text{Mn}^{2+}$  ions in strongly defective ZnS single crystals, we could demonstrate that the local axial crystal field component at the substitutional  $\text{Mn}^{2+}$  ion is due to the presence of a neighboring extended lattice defect (ELD) in the form of a stacking fault or twin. We have also concluded that the ELD play an essential role in the incorporation and localization in the cubic ZnS NCs lattice of the  $\text{Mn}^{2+}$  impurity ions. Based on previously published EPR results it is proposed that a similar extended lattice defects assisted (ELDA) mechanism of impurities incorporation is acting in the case of other cubic II-VI semiconductor NCs doped with  $\text{Mn}^{2+}$  ions as well.

## 2. Experimental

The QDs of cZnS:Mn were synthesized by precipitation in a surfactant-assisted liquid-liquid reaction, at room temperature [12, 13]. In the initial stage 0.2% mol manganese acetate [ $\text{Mn}(\text{CH}_3\text{COO})_2 \cdot 4\text{H}_2\text{O}$ ] has been added to a zinc acetate

$[Zn(CH_3COO)_2 \cdot 2H_2O]$  solution and further mixed for 15 minutes. Afterwards the resulting solution was co-precipitated with sodium sulfide  $[Na_2S \cdot 9H_2O]$  in the presence of Tween 20 (polyoxyethylene sorbitan monolaurate), a nontoxic additive used in the food industry. In the post synthesis steps the precipitate was filtered, washed with bi-distilled water and methanol and dried at  $50^\circ C$  for 24 h. The concentration of the  $Mn^{2+}$  ions at isolated sites in the nanocrystalline ZnS has been estimated from EPR measurements, using concentration standards of  $MgO:Mn^{2+}$  crystalline powders, to be in the 2-400 ppm range.

The X-ray diffraction (XRD) characterization of the resulting material shows (Figure 1a) the formation of a mesoporous structure consisting of nanocrystals of ZnS with cubic (sphalerite) structure of 1.9 nm average diameter. The transmission electron microscopy (TEM) images and electron diffraction (ED) patterns (Figure 1b) confirmed the above conclusions, revealing the details of the structure of the mesoporous material with walls consisting of cubic ZnS nanocrystals with uniform size, of 2.1 nm average diameter. This value was obtained by measuring the size of 259 nanocrystals.

The EPR investigations were performed on QDs of cZnS doped with 0.2% mol  $Mn^{2+}$ , self-assembled into a mesoporous structure, which were prepared at room temperature (RT) by a surfactant-assisted liquid-liquid reaction [12]. The preparation procedure, as well as the results of structural and preliminary X-band EPR and optical characterization of the presently investigated sample batch was reported elsewhere [13, 14].

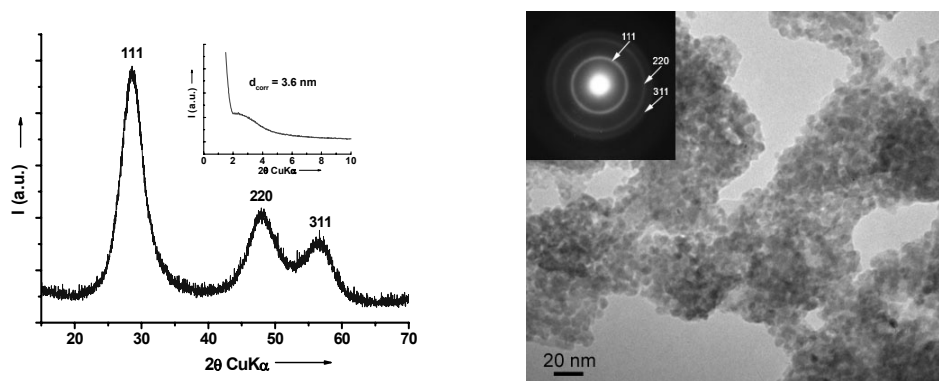


**Fig. 1.** The microstructure of the presently investigated cZnS:Mn QDs as revealed by: Left - wide-angle XRD diffractogram. Inset - the low angle range reflecting the mesoporous structure of the resulting nanomaterial; and (b) Right - TEM image revealing the mesoporous morphology of the cZnS:Mn sample. Inset - the corresponding ED pattern indexed with the cubic (sphalerite) ZnS structure.

The X (9.8 GHz)- and Q (34 GHz)-band measurements were performed at RT on Bruker EMX-plus and ELEXSYS 500Q spectrometers, respectively, at the

Research center for advanced ESR techniques (CetRESav - <http://cetresav.infim.ro/>) from NIMP. High frequency W (95 GHz)-band measurements were performed on a Bruker E600 spectrometer from the Department of Physics – ECMP, University of Antwerp, Belgium. The SH parameters were determined by lineshape simulations and fitting procedures with the SIM specialized program graciously provided by Prof. H. Weihe of the University of Copenhagen and the publicly available EasySpin v. 3.1 program.

### 3. Results and Discussion

We have identified in the preliminary X-band EPR investigations of the cZnS:Mn QDs the presence of a substitutional Mn<sup>2+</sup> center, called Mn(I), which does not change its concentration by thermal treatments, and two surface centers, called Mn(II) and Mn(III) [13, 15]. The Mn(III) centers were found to transform into Mn(II) centers during heating, by the temperature activated desorption of water molecules from the nanocrystals surface [14]. Figure 2 illustrates such a situation, where the X- and Q – band EPR spectra from samples of the same batch, but with a different thermal history, exhibit a different relative concentration/ lines intensity of the Mn(II) and Mn(III) centers. The transition fields attributed to the Mn(I), Mn(II) and Mn(III) centers are marked with vertical lines, namely 6 allowed ( $M_s: -1/2 \leftrightarrow 1/2, \Delta M_I = 0$ ) and 10 forbidden ( $M_s: -1/2 \leftrightarrow 1/2, \Delta M_I = \pm 1$ ) hyperfine transitions for the Mn(I) centers and only the 6 allowed hyperfine transitions for the Mn(II) and Mn(III) centers. These observed features are typical for the Mn<sup>2+</sup> ions in crystalline powders [3, 16]. One can see that in the case of the left hand side X-band spectrum the intensities of the lowest magnetic field lines from the two surface centers are comparable. Meanwhile, in the other spectrum from a sample with a different history (recorded in the Q-band), the concentration/ lines intensity of the Mn(II) surface center is much smaller compared to the concentration/ lines intensity of the Mn(III) surface center.

The EPR spectrum of the Mn<sup>2+</sup> centers in nanocrystalline cZnS is described by the following SH, with usual notations [3]:

$$\mathbf{H} = \mu_B \tilde{\mathbf{S}} \hat{\mathbf{g}} \tilde{\mathbf{B}} + \tilde{\mathbf{S}} \hat{\mathbf{A}} \tilde{\mathbf{I}} + \mathbf{CF} \quad (1)$$

Here the first two terms represent the main interactions of the  $S = 5/2$  electron spin +with the external magnetic field and the hyperfine interaction with the  $I = 5/2$  nuclear spin of the <sup>55</sup>Mn (100% abundance) isotope, respectively. The last zero field splitting (ZFS) term describes the interaction of the electron spin with the local crystal field, characterized in the case of a local cubic symmetry, typical for cubic ZnS single crystals, by the  $a$  parameter and in the case of lower symmetry by additional axial and rhombic ZFS terms with the  $D$  and  $E$  parameters, respectively [3].

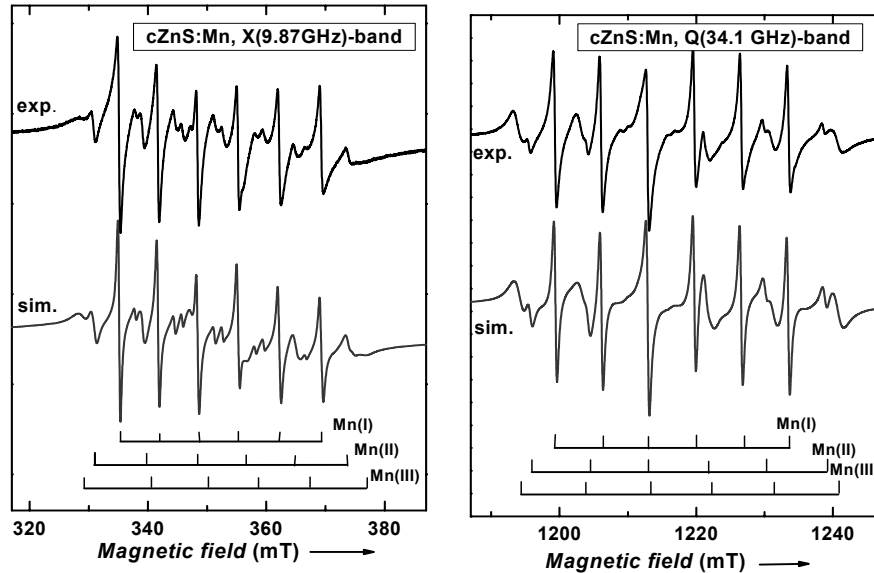


**Fig. 2.** The X- and Q-band EPR spectra of cZnS:Mn QDs powder samples with a different thermal history. The upper curves represent the experimental spectra while the lower curves are, in each case, the sum of the simulations of the Mn(I), Mn(II) and Mn(III) spectra calculated with the SH parameters given in Table 1.

We have been able to obtain accurate SH parameter values for the  $Mn^{2+}$  centers in the cZnS:Mn QDs (Table 1) by fitting both low and high frequency experimental EPR spectra with line shape simulations which took into account the forbidden transitions and the line broadening effects, both strongly influenced by the non-cubic crystal ZFS terms. The increased accuracy of the SH parameters determinations was also possible due to the narrower lines exhibited by our EPR spectra, i.e. 0.4 mT linewidth for the Mn(I) center in the X-band, as compared to the best reported value of 0.6 mT [7]. The two steps procedure for determining the SH parameters was described in Ref. [17]. In the first step the  $g$  and  $A$  parameters were determined with high accuracy from fitting the line positions in the Q-band spectrum with transition fields calculated with a SH consisting of only the first two terms of SH (1). At higher magnetic fields the contributions of the ZFS terms to the line positions were found to be negligible (within the experimental errors). An accurate value for the  $D$  parameter was further determined from fitting the line shape of the X-band spectrum, more sensitive to the ZFS terms. One should also mention that in the case of a local axial crystal field, the cubic fourth order ZFS term characterized by the  $a$ -parameter should be in principle replaced by an axial fourth order term characterized by the  $a-F$  parameter [3]. However, because of the small values of the fourth order ZFS terms, the strong line broadening effects, included as fluctuations in the ZFS parameter values to fit both X- and Q-band spectral line shapes, were practically wiping out their contribution, making it

impossible to determine accurate values. Therefore, in our calculations we considered the cZnS single crystal value  $a = 7.987 \times 10^{-4} \text{ cm}^{-1}$  [11].

**Table 1.** The SH parameters at RT of the substitutional  $\text{Mn}^{2+}$  ions in cZnS:Mn QDs, called the Mn(I) centers, as well as of the surface Mn(II) and Mn(III) centers, are presented and compared with previously reported values in cZnS NCs and similar values from substitutional  $\text{Mn}^{2+}$  ions in ZnS single crystals. The hyperfine ( $A$ ) parameter and the cubic ( $a$ ), axial ( $a-F$ ,  $D$ ) and rhombic ( $E$ ) ZFS parameters are given in  $10^{-4} \text{ cm}^{-1}$  units.

Lattice host/ $\text{Mn}^{2+}$ center	Ref.	$g$	$A$	$ D $	$a$
cZnS:Mn QDs / Mn(I)	[17,18 ]	2.0022	-63.7	41	7.987
cZnS:Mn QDs / surface Mn(II)	[17,18]	2.0012	-80.5	~10-80	
cZnS:Mn QDs / surface Mn(III)	[17,18]	2.0009	-86.8	~ 10-90	
cZnS:Mn NCs/ NC1	[5]	2.003	-64.5		
cZnS:Mn NCs / SI	[6]	2.0010	-63.9	1.0	
ZnS:Mn NCs/ center I	[7, 8]	2.0024	-64.5	91.0	
cZnS:Mn NCs /samples 1 and 2	[9]	$g_{xx} = 2.0064$ $g_{yy} = 2.0064$ $g_{zz} = 2.0066$	$A_{xx} = -63.9$ $A_{yy} = -64.0$ $A_{zz} = -64.4$	37.4 $ E  = 12.47$	
cZnS:Mn NCs / Ib	[10]	$g_{\square} = 2.0075$ $g_{\parallel} = 2.0040$	$A_{\square} = -63.8$ $A_{\parallel} = -65.2$	37.4 $ E  = 12.47$	
cZnS:Mn single crystal / substitutional $\text{Mn}^{2+}$	[11]	2.00225	-63.88	0	7.987
Mixed polytype ZnS:Mn single crystal / trig. $\text{Mn}^{2+}$ (PN center)	[20,21]	2.0018	-64.9	36.1	7.35 $a-F = 7.4$
Microtwined cZnS:Mn single crystal / trig. $\text{Mn}^{2+}$ (PN center)	[22]	2.0016	-64.5	37.85	$a-F = -7.5$

The quality of the fitting with the experimental spectra (see Fig. 2) demonstrates that the substitutional Mn(I) center EPR spectra are well described by the SH (1), which includes, besides the cubic terms with  $g$  and  $A$  values very close to those found in the cZnS single crystals, the axial ZFS term with  $|D| = 41 \times 10^{-4} \text{ cm}^{-1}$ . The resulting SH parameters presented in Table 1 are also in good agreement with the

values we have previously obtained from the analysis of the X- and W-band EPR spectra [17]. As discussed in Ref. [18], which was dedicated to their structure and properties, the two surface Mn(II) and Mn(III) centers represent  $Mn^{2+}$  ions localized at the surface of the cZnS:Mn NCs in partly oxidized areas, without or with an adsorbed water molecule attached, respectively.

The additional axial ZFS term involved in describing the EPR spectrum of the substitutional  $Mn^{2+}$  ions in the investigated cZnS:Mn QDs is related with the presence of a local axial crystal field component (or local distortion of the lattice) at the cation  $Zn^{2+}$  site, with otherwise pure cubic ( $T_d$ ) symmetry in the bulk cZnS single crystals [11]. The resulting value of the  $D$  parameter suggests a unique configuration with a neighboring defect, either as an unintentional impurity, or as an intrinsic lattice defect. A neighboring natural impurity seems unlikely, because the estimated  $\sim 200$  ppm concentration of  $Mn^{2+}$  ions in our cZnS:Mn QDs is too high compared to the trace impurity levels in the starting materials. A neighboring intrinsic point defect (vacancy/interstitial) is also unlikely, in view of the similar electrical charges and close radii of the  $Mn^{2+}$  impurity and substituted  $Zn^{2+}$  cation. Also, a local axial crystal field resulting in a ZFS term with finite  $D$  parameter value could not be caused by the presence of size induced strains in the QDs [19]. The random character of such strains can only contribute to the experimentally observed inhomogeneous broadening of the EPR lines in QDs.

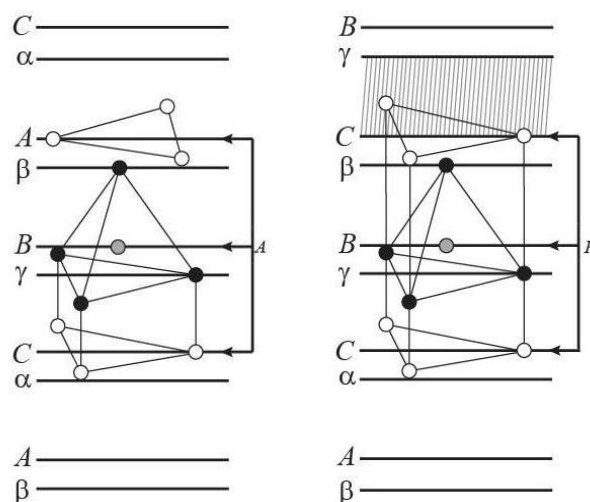


**Fig. 3.** The local structure at the substitutional  $Mn^{2+}$  ions, shown in the left hand side drawing for a pure cubic ZnS single crystal lattice and in the right hand side drawing for a  $Zn^{2+}$  lattice site perturbed by the presence of a neighboring stacking fault (shaded area) resulting in a trigonal distortion at the  $Mn^{2+}$  ion (grey), called the PN center. In both drawings the  $Zn^{2+}$  cations and  $S^{2-}$  anions are represented by open and filled circles, respectively, aligned as {111} layers, and the substitutional  $Mn^{2+}$  at a  $Zn^{2+}$  cation site by a shaded circle.

A more plausible explanation is obtained by comparing the SH parameters of the substitutional Mn(I) center with the corresponding parameters of the substitutional Mn<sup>2+</sup> (PN) center with local trigonal symmetry and very close SH parameter values, reported in mixed polytype ZnS or micro-twined cZnS single crystals [20-22]. As shown from correlated theoretical calculations and optical investigations, the PN center consists of a substitutional Mn<sup>2+</sup> ion at a Zn<sup>2+</sup> site where the normal stacking sequence of layers along the sphalerite <111> direction (equivalent to *c*-axis in wurtzite), at the third order neighboring ligands, was changed by the gliding of a neighboring layer due to a stacking fault or twin [20-22]. From the close values of the axial ZFS parameter *D* of the PN center in ZnS:Mn single crystals and the Mn(I) center in the cZnS QDs (see Table 1) one concludes that in the later case the substitutional Mn<sup>2+</sup> impurity is localized in a {111} layer, which contains the Mn<sup>2+</sup> ion and its tetrahedrally coordinating sulfur ligands, lying next to a stacking fault or twin. The resulting PN center–type configuration, illustrated on the right hand side in Figure 3 is characterized by the presence of a local axial (trigonal) crystal field at the substitutional Mn<sup>2+</sup> impurity ion, which leads to the additional axial ZFS term in the SH (1). The small differences in the measured SH parameters of the substitutional Mn(I) centers in the cZnS QDs and of the PN center in the defective ZnS single crystals (see Table 1) are attributed to experimental errors and/or possible slight differences in the arrangement of the first neighboring ligands in the single crystals and nanocrystals, respectively.

In order to confirm the validity of the proposed ELD model of localization of the Mn<sup>2+</sup> ions in the cZnS:Mn QDs we had to prove that a rather large concentration of such defects exists in the investigated QDs. In crystals with a sphalerite structure planar stacking defects such as stacking faults and twins are known to occur along the {111} planes. To reveal the stacking defects in the cZnS:Mn QDs we performed high resolution transmission electron microscopy (HRTEM) investigations. One should mention that the atomic structure of the extended defects can be imaged by HRTEM only if the defects exhibit translation symmetry along the viewing direction. For crystals with sphalerite structure this condition is fulfilled along the [110] viewing direction. Figure 4 shows HRTEM images of very thin parts of cZnS:Mn QDs which were extracted from a cZnS:Mn nanocrystalline sample previously investigated by EPR spectroscopy. As shown in the picture some of the cZnS QDs exhibit planar extended defects such as twins (T) or stacking faults (SF), marked by arrows. Any substitutional impurity localized in a cation site next to these defects (Figure 3) will be therefore in a disturbed neighborhood, with regard to the perfect cubic lattice, in agreement with our EPR investigations.

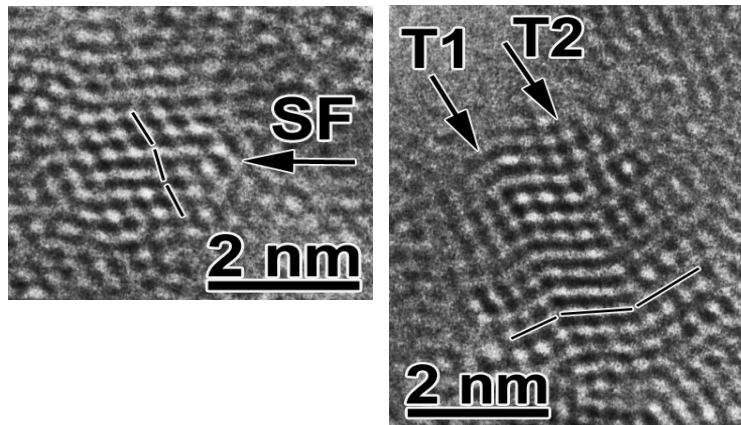


**Fig. 4.** HRTEM image of cZnS:Mn QDs from a sample previously investigated by EPR spectroscopy revealing in some crystallites (marked by arrows) planar defects such as twin interfaces (T) and stacking faults (SF).

By examining several HRTEM images we found out that a rather large amount (at least 30%) of the cZnS:Mn QDs oriented along [110] contain planar extended defects in the form of stacking faults and twins. Considering that the ZnS:Mn nanocrystallites are arbitrarily oriented in the investigated sample it results that a corresponding fraction of them contain such extended defects, which represents more than enough to explain the observed concentration of the substitutional Mn(I) centers. The observation of the extended defects by HRTEM also confirms the simulation results based on a Debye function analysis, which has shown [23] that the presence in the small cZnS nanocrystals of extended defects in the form of twins is essential for an accurate fitting of the experimental XRD patterns.

#### 4. Conclusions

Considering that no sizable amount of substitutional  $Mn^{2+}$  ions localized at unperturbed  $Zn^{2+}$  cation sites with  $T_d$  symmetry could be identified in our investigated cZnS:Mn QDs, it results that the ELDs in the form of stacking faults and twins are essential in the localization of the  $Mn^{2+}$  ions in the cZnS QDs.

The presence of a local axial ZFS term of comparable magnitude in the SH describing the EPR spectrum of substitutional  $Mn^{2+}$  ions has been reported in cubic CdS nanocrystals [24] as well and occurs very likely in ZnSe:Mn nanocrystals, which also exhibit forbidden hyperfine transitions in the  $Mn^{2+}$  EPR spectrum [25]. Therefore, it is reasonable to assume that a similar localization of the substitutional  $Mn^{2+}$  ions involving a neighboring extended defect is valid for other cubic II-VI semiconducting nanocrystals doped with  $Mn^{2+}$  and possible with other divalent cations such as  $Co^{2+}$ .

The localization of the substitutional  $Mn^{2+}$  in the II-VI semiconductor QDs next

to ELDs has some very important fundamental and applicative implications. Thus, it demonstrates that the ELDs play an essential role in the incorporation of  $Mn^{2+}$  and possibly of other divalent impurities in the very small nanocrystals, which usually do not exhibit well defined facets, considered [2] essential for activating the diffusion assisted incorporation of impurities. On the other hand, it is well known that extended defects such as steps on the surfaces or dislocations, which emerge when the extended defects intersect the nanocrystals surface, are very likely to "attract" impurities [26]. Therefore, one expects the doping to be mainly controlled by the trapping of impurities at the steps and dislocations at the surface of the growing nanocrystals, a mechanism which was not considered up to now.

The large fraction of planar extended defects observed in our investigated cZnS:Mn QDs samples can also explain the relatively high fraction of the doping  $Mn^{2+}$  impurities (more than 10%) found in the investigated cubic II-VI semiconductor QDs [25] and still unexplained, as well as the high concentrations of  $Mn^{2+}$  impurities, including the formation of impurity aggregated states at higher dopant concentrations, previously reported in ZnS nanocrystals of comparable size [6-8, 10].

We should also mention that, according to our results, at higher dopant concentrations one expects the impurities to aggregate preferentially in  $\{111\}$  planes parallel to the extended defects, resulting in properties specific for 2D systems, a subject to be further investigated.

In summary, we conclude that the high doping levels of  $Mn^{2+}$  ions in the cubic II-VI semiconductor QDs prepared by colloidal growth are very likely controlled by the proposed mechanism of extended lattice defects assisted (ELDA) incorporation of impurities. This mechanism also explains the reported localization of  $Mn^{2+}$  impurities at cation sites situated next to an extended lattice planar defect, resulting in a local crystal lattice deformation at the impurity ion, which should also be taken into consideration in the description of the local quantum states and resulting optical, electrical and magnetic properties.

**Acknowledgements.** The present research was supported by CNCSIS-UEFISCSU, project number PN-II-ID-523/2008, and ANCS in the frame of the project Nucleu PN09-450102.

## References

- [1] ERWIN S.C., ZU L., HAFTEL M.I., EFROS A.L., KENNEDY T.A. and NORRIS D.J., *Nature* **436**, pp. 91–94, 2005.
- [2] NORRIS D.J., EFROS A.L. and ERWIN S.C., *Science* **319**, pp. 1776–79, 2008.
- [3] ABRAGAM A. and BLEANEY B., *Electron Paramagnetic Resonance of Transition Ions*, Clarendon Press, Oxford, 1970.
- [4] HU H. and ZHANG W., *Opt. Mat.* **28**, pp. 536–50, 2006.
- [5] KENNEDY T.A., GLASER E.R., KLEIN P.B. and BHARGAVA R.N., *Phys.Rev. B* **52**, pp. R14356–59, 1995.

- [6] BORSE P.H., SRINIVASA D., SHINDE R.F., DATE S.K., VOGEL W. and KULKARNI S.K., *Phys. Rev. B* **60**, pp. 8659–64, 1999.
- [7] IGARASHI T., IHARA M., KUSUNOI T., OHNO K., ISOBE T. and SENNA M., *J. Nanoparticles Res.* **3m**, pp. 51–56, 2001.
- [8] IGARASHI T., ISOBE T. and SENNA M., *Phys. Rev. B* **56**, pp. 6444–45, 1997.
- [9] GONZALEZ BEERMANN P.A., MCGARVEY B.R., MURALIDHARAN S. and SUNG R.C.W., *Chem. Mater.* **16**, pp. 915–18, 2004.
- [10] GONZALEZ BEERMANN P.A., MCGARVEY B.R., SKADTCHENKO B.O., MURALIDHARAN S. and SUNG R.C.W., *J. Nanoparticles Res.* **8**, pp. 235–41, 2006.
- [11] NISTOR S.V. and STEFAN M., *J. Phys.: Condens. Matter* **21**, 145408 (7pp), (2009) and references cited therein.
- [12] NISTOR L.C., MATEESCU C.D., BIRJEGA R. and NISTOR S.V., *Appl. Phys. A* **92**, pp. 295–301, 2008.
- [13] NISTOR S.V., NISTOR L.C., STEFAN M., MATEESCU C.D., BIRJEGA R., SOLOVIEVA N. and NIKL M., *Superlatt. and Microstruct.* **46**, pp. 306–11, 2009.
- [14] NISTOR S.V., STEFAN M., NISTOR L.C., MATEESCU C.D., BIRJEGA R., *J. Nanosc. Nanotechn.* **10**, pp. 1–6, 2010.
- [15] NISTOR S.V., NISTOR L.C., STEFAN M., GHICA D., MATEESCU C.D. and BIRJEGA R., *Rom. Rept. Phys.* **62**(2), pp. 319–28, 2010.
- [16] RUBIO J.O., MUNOZ P.E., BOLDU O.J., CHEN Y. and ABRAHAM M.M., *J. Chem. Phys.* **70**, pp. 633–38, 1979.
- [17] NISTOR S.V., STEFAN M., NISTOR L.C., GOOVAERTS E., and TENDELOO Van G., *Phys. Rev. B* **81**, 035336 (6pp), 2010.
- [18] STEFAN M., NISTOR S.V., GHICA D., MATEESCU C.D., NIKL M., and KUCERKOVA R., *Phys. Rev. B* **83**, 045301 (11 pp), 2011.
- [19] QADRI S.B., SKELTON E.F., HSU D., DINSMORE A.D., YANG J., GRAY H.F. and RATNA B.R., *Phys. Rev. B* **60**, pp. 9191–939, 1999.
- [20] LAMBERT B., BUCH T. and CLERJAUD B., *Sol. State Commun.* **10**, pp. 25–27, 1972.
- [21] BUCH T., CLERJAUD B., LAMBERT B. and KOVACS P., *Phys. Rev. B* **7**, pp. 184–91, 1973.
- [22] YAKUNIN A., SHTAMBAR I.V., KUSHNIR A.S. and OMELCHENKO S.A., *Russian Phys. J.* **16**, pp. 1375–79, 1973.
- [23] VOGEL W., BORSE P.H., DESHMUCK N. and KULKARNI S.K., *Langmuir* **16**, pp. 2032–37, 2000.
- [24] COUNIO G., ESNOUF S., GASCOIN T. and BOILOT J.P., *J. Phys. Chem.* **100**, pp. 20021–26, 1996.
- [25] NORMAN Jr.T.J., MAGANA D., WILSON T., BURNS C., ZHANG J.Z., CAO D. and BRIDGES F., *J. Phys. Chem. B* **107**, pp. 6309–17, 2003.
- [26] AMELINCKX S., *The Direct Observation of Dislocations*. In *Solid State Physics: Advances in Research and Applications*. Suppl. **6**, pp. 55–89, Seitz F. & Turnbull D., Eds., Academic Press: New York, 1964.